Study of Constant Current-Constant Voltage Output Wireless Charging System Based on Compound Topologies

Linlin Tan[*],[**],[***], Shulei Pan[*], Changfu Xu[****], Changxin Yan[*], Han Liu[*], and Xueliang Huang[†],[**]

[†],[*]School of Electrical Engineering, Southeast University, Nanjing, China
[**]Jiangsu Key Laboratory of Smart Grid Technology and Equipment, Nanjing, China
[***]Zhifang Engineering Design Co. Ltd, Nanjing, China
[****]Jiangsu Electric Power Company Research Institute, Nanjing, China

Abstract

Wireless power transfer (WPT) technology has the advantages of intelligence and facilitation. This paper designs a WPT system applied to battery charging and provides a strategy which switches from the constant current (CC) charging mode to constant voltage (CV) charging mode. The LCL-LCL topology is used to realize the CC output, while the LCL-S (series compensation) topology is used to realize the CV output. The main factor affecting the output characteristics is extracted by analyzing the two topologies above. Based on the main factor, this paper puts forward a modified way to design the system. In addition, on-line monitors for the battery and switches are placed at receiving side, which avoids the need for introducing an information interaction module into the system. Therefore, the complexity of the controlling system is reduced. Finally, simulation and experimental analyses are carried out to verify the correctness of the compound topologies.

Key words: Constant current (CC) output, Constant voltage (CV) output, Switching strategy, Wireless power transfer (WPT)

I. INTRODUCTION

Wireless power transfer (WPT) technology [1]-[4] has a lot of advantages when compared to traditional wire transmission, and it has been widely applied to electric vehicles (EVs), intelligent appliances, aerospace applications and industrial robots [5]-[8]. There have been a lot of researches done on power transfer problems [9]. However, due to the fact that energy transmission and storage are equally important, the problems assoicated with efficient energy storage systems should be solved when WPT technology is used to transmit power. The most common equipment for energy storage is the lithium-ion battery. For

lithium-ion batteries, the charging process usually consists of two main stages [10]: a constant-current (CC) charging stage and a constant-voltage (CV) charging stage.

In general, in order to realize CC and CV charging for lithium-ion batteries, special DC converters need to be designed [11]. There is no doubt that this increases both the cost of system and the technical complexity. Some studies have found that with the mutual inductance unchanged or changed a tiny amount, a magnetic coupling resonant WPT system can realize CC and CV outputs by changing the topologies. Thus, a method to achieve CC and CV outputs for battery charging by changing the topologies is of preference since this can diminish much stress on the following circuit modules.

To realize the CC and CV outputs by utilizing a topological transformation, a series of studies have been conducted [12]-[17]. In [12], the authors analyzed the CV output in a WPT system with parallel-series (PS) compensation. In addition, a coil array has been designed to charge a mouse with CV regardless of position variations. Auvigne proposes a dual topology transition with

series-series (SS) and series-parallel (SP) to realize CC and CV charging, respectively [13]. Although the system maintains the same frequency during the switching process, the receiving coil needs to be replaced leading to an increase in the volume of the wireless equipment. Huang designs a SS compensation to realize the CC and CV outputs at two different frequencies [14]. In this design, the topology remains unchanged during the process, which simplifies the complexity of the system. However, the input impedance is inductive when operating in the CV mode. Excessive reactive power degrades the transfer efficiency. In [15], switches at the transmitting side are controlled by monitoring the voltage of batteries at the receiving side to change the SS compensation to PS compensation. During the process of switching from the CC mode to the CV mode, the input voltage and system frequency remain unchanged. However, this adds an information interaction module between the transmitting side and the receiving side.

In [18]-[21], using LCL topological connection at the transmitting side can keep the current in the transmitting coil constant with a fixed source voltage. According to the mutual inductance model theory, a constant voltage source, which is directly influenced by the input voltage, is introduced into the receiving side of a WPT system. Therefore, an LCL topology is chosen as the topology at the transmitting side. By reasonably selecting the topology at the receiving side, the LCL-LCL topology realizing the CC output and the LCL-S topology realizing the CV output are designed. In addition, this paper studies the output characteristics of these topologies and extracts the main factors. And a system design scheme based on the above two topologies is given.

The contents of this paper are arranged as follows. In section II, an ideal LCL model and the selection of the topology at the receiving side are studied. In section III, the influence of the inner resistances of the compensation inductors and energy transmission coils on the output characteristics is analyzed comparatively. In section IV, a switching strategy from the CC mode to the CV mode is provided. To ensure that the charging current in the CC mode and the charging voltage in the CV mode satisfy the system requirements, a universal way to design the system parameters is also proposed. Finally, the validity and accuracy of the analysis and design are verified by simulations and experiments.

II. TOPOLOGY SELECTION

A. Topology Selection at the Transmitting Side

Without considering the inner resistances, the ideal LCL circuit is shown in Fig. 1. In Fig. 1, U_{in} is the input power. L_X and L_P are inductors. C_P is the compensation capacitor, and Z is the equivalent load. In addition, $L_X = L_P$ and $\omega_0 = 1/\sqrt{L_p C_P}$.
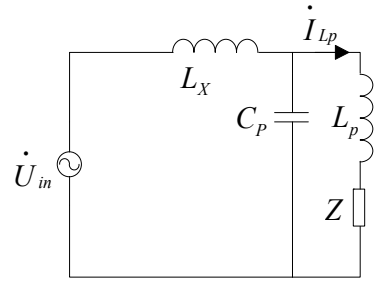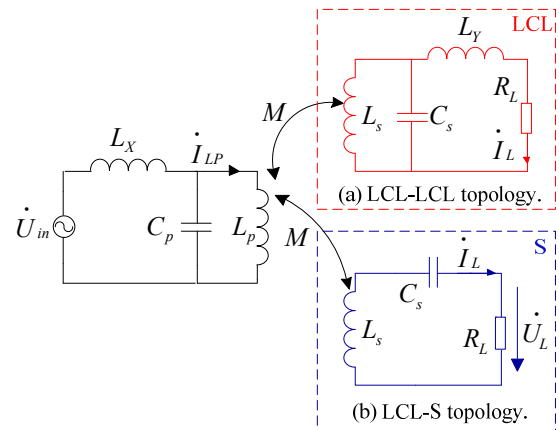

Fig. 1. LCL circuit schematic.

(a) LCL-LCL topology.

(b) LCL-S topology.

Fig. 2. Equivalent circuits of WPT systems with different compensation topologies.

Therefore, the current I_{Lp} flowing through the load Z is $U_{in}/(j\omega_0 L_P)$ [21].

It is obviously that I_{Lp} is load-independent, and that it is concerned with U_{in}, L_P and ω_0. The above analysis shows that I_{Lp} is constant when the parameters L_P, ω_0, and U_{in} are unchanged. If an LCL circuit is introduced into a WPT system and an LCL circuit is selected as the topology at the transmitting side, the controlled voltage source $j\omega_0 M I_{Lp}$ is equal to being added at the branch of the receiving coil, which is only related to U_{in} without being influenced by the parameters at the receiving side.

B. Topology Selection at the Receiving Side

To obtain CC and CV outputs, the receiving coil and compensation capacitor at the receiving side need to be further studied. Depending on the type of connection, an LCL topology and an S topology are designed, as shown in Fig. 2.

In Fig. 2, the LCL topology is chosen as the transmitting topology so that the branch current of L_p is constant. The LCL circuit is employed at the receiving side in Fig. 2(a). When $L_Y = L_S$ and $\omega = \text{sqrt}(1/L_s C_s)$, I_L can be calculated as:

$$\dot{I}_L = \frac{M \dot{U}_{in}}{j\omega L_S L_P} \tag{1}$$

Obviously, I_L is load-independent and is independent of load characteristics. Meanwhile, in Fig. 2(b), the S circuit is employed at the receiving side. U_L is also load-independent.
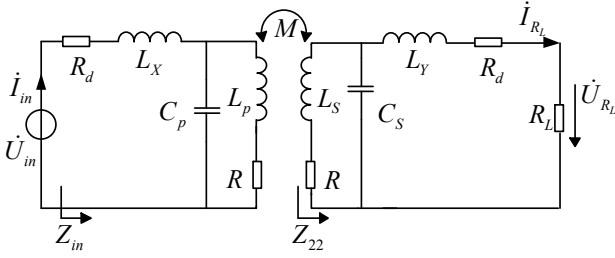
Fig. 3. LCL-LCL topology considering the inner resistances.

Fig. 4. LCL-S topology considering the inner resistances.

$$\dot{U}_L = \frac{M\dot{U}_{in}}{L_P} \tag{2}$$

In conclusion, the LCL-LCL topology is chosen to obtain the CC output, and the LCL-S topology is used to obtain the CV output. The input impedances of the LCL-S topology and the LCL-LCL topology are computed.

$$Z_{in} = \frac{L_P^2 R_L}{M^2} \quad \text{(LCL-S)} \tag{3}$$

$$Z_{in} = \frac{L_P L_S}{\omega^2 M^2 C_S C_P R_L} \quad \text{(LCL-LCL)} \tag{4}$$

It can be seen from (3) and (4) that the input impedances are purely resistive. This means that a zero phase angle (ZPA) is achieved between the input voltage and the input current. This brings a lot of advantages for the inverter and can easily realize ZVS or ZCS control.

III. THE ANALYSIS OF A WPT SYSTEM

A. Topology of the CC Mode by Considering the Inner Resistances of Inductors

The LCL-LCL and LCL-S topologies in section II are obtained under ideal conditions. However, the inner resistance is one of the main factors that affects the quality factor of a coil. Therefore, it is necessary to analyse these factors. The equivalent circuit of the LCL-LCL is shown in Fig. 3. The inner resistances of L_X and L_Y both are R_d. The transmitting coil L_p and receiving coil L_S are the same. The inner resistances of L_p and L_S are both R. In addition, $C_P = C_S = C$, $L_X = L_Y = L_P = L_S = L$, $\omega = \text{sqrt}(1/LC)$.

Therefore, in Fig. 3, the impedance at the receiving side is:

$$Z_{22} = R + \frac{L}{(R_d + R_L)C} \tag{5}$$

In addition, the reflected impedance Z_{ref} is equal to $(\omega^2 M^2)/Z_{22}$. Therefore, the input impedance Z_{in} and input current I_{in} can be calculated.

$$Z_{in} = R_d + \frac{L}{C(R + Z_{ref})} \tag{6}$$

$$\dot{I}_{in} = \frac{C\dot{U}_{in}(R + Z_{ref})}{CR_d(R + Z_{ref}) + L} \tag{7}$$

Thus, the load current I_{RL} can be obtained.

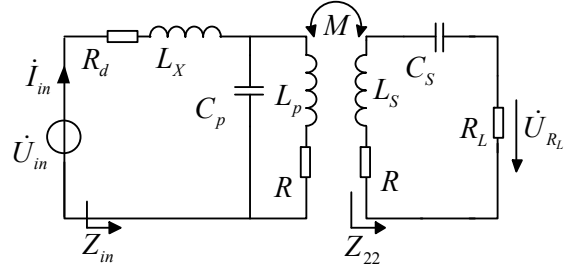$$\dot{I}_{RL} = \lambda \frac{M\dot{U}_{in}}{j\omega L^2} \tag{8}$$

By comparing this with (1), λ denotes the correlation coefficient.

$$\lambda = \frac{L}{L + C[R_d(R + Z_{ref}) + (R_L + R_d)(R + \frac{C}{L}R_d R(R + Z_{ref}))]} \tag{9}$$

From (9), $k = d\lambda/dR_L$. When calculating, $k < 0$ and $\lambda < 1$. Therefore, because of the inner resistances, when the value of R_L increases, the value of I_{RL} decreases. The constant output characteristic is affected. Qualitative and quantitative analysis is needed to analyse the effect. Since $\text{Im}(\dot{I}_{in}) = 0$, for the LCL-LCL topology in Fig. 3, the inner resistance does not change the characteristic of the input impedance.

B. Topology of the CV Mode by Considering the Inner Resistances of Inductors

In the CV mode, the LCL topology is still used as the transmitting side of a WPT system, while series compensation is applied for the receiving side in Fig. 4. Similarly, $Z_{22} = R + R_L$. Therefore, the reflected impedance $Z_{ref,s}$ is equal to $(\omega^2 M^2)/Z_{22}$. The input impedance Z_{in} and input current I_{in} can be calculated.

$$Z_{in} = R_d + \frac{L}{C(R + Z_{ref,s})} \tag{10}$$

$$\dot{I}_{in} = \frac{C\dot{U}_{in}(R + Z_{ref,s})}{CR_d(R + Z_{ref,s}) + L} \tag{11}$$

Thus, the voltage U_{RL} of R_L can be obtained. The following is obtained:

$$\dot{U}_{RL} = \lambda_s \frac{M\dot{U}_{in}}{L} \tag{12}$$

where λ_S denotes the correlation coefficient between (2) and (12).

$$\lambda_s = \frac{R_L}{R + R_L} \cdot \frac{1}{1 + CR_d(R + Z_{ref,s})/L} \tag{13}$$

From (13), $d\lambda_s/dR_L > 0$. The value of λ_S increases progressively and tends to 1. According to $\text{Im}(\dot{I}_{in}) = 0$,
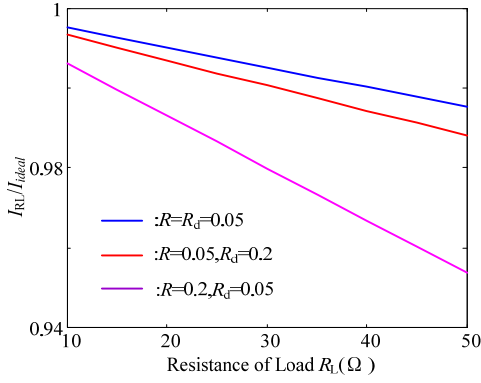
Fig. 5. Effect of the inner resistances on the output current in the LCL-LCL topology.
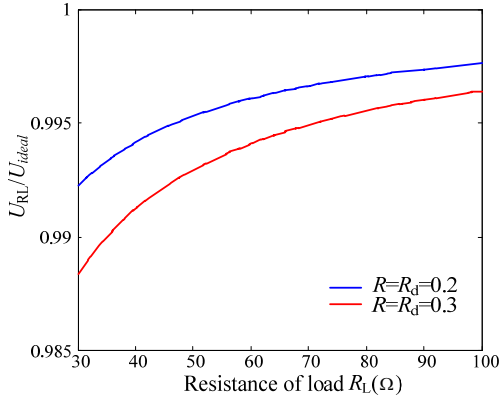

Fig. 6. Effect of the inner resistances on the output voltage in the LCL-S topology.

the input voltage still has the same phase as the input current.

C. The Simulation in the CC Mode

In order to study the effect above in both qualitative and quantitative ways, simulations of these two topologies are built, and the simulation parameters are given in Table I.

In the CC mode, according to (1), the ideal constant current I_{ideal} is obtained. To quantify the deviation of the ideal output,the output current considering the inner resistances is normalized by comparing it with I_{ideal}. In Fig. 5, the value of the output current I_{RL} decreases when R_L increases. k is used to describe the deviation of the ideal output. For instance, $k_{0.05,0.2}$ denotes the slope of curve when $R=0.05\Omega$ and $R_d=0.2\Omega$. In Fig. 5, $|k_{0.05,0.2}|<|k_{0.2,0.05}|$. Thus, when R_L is the same, the impact on the output deviation brought by R is much larger than that caused by an R_d of the same value. Therefore, by extracting the main factor and ignoring the side effect, the calculation of λ can be simplified as $\lambda=1/(1+RR_LC/L)$. The relationship between U_{in} and I_{RL} is modified as:

$$\dot{I}_{R_L} = \frac{M\dot{U}_{in}}{j\omega LCRR_L + j\omega L^2} \tag{14}$$

In order to obtain a constant current which is consistent

TABLE I
SIMULATION PARAMETERS

Parameter	Value
f	64.3kHz
L_p, L_s, L_X, L_Y	12μH
C_p, C_s	0.51μF
M	2.5μH
U_{in}	26V

with the preset one in the CC mode, R is needed to be taken into consideration when designing the system parameters.

D. The Simulation in the CV Mode

Similarly, the effect of the inner resistances on the CV output with the LCL-S topology is shown in Fig. 6. The output voltage considering the inner resistances is normalized by comparing it with the value U_{ideal} calculated by (2).

It is obvious that increasing the values of R and R_d results in a decrease of the output voltage U_{RL}. In addition, U_{RL} increases with the increase of R_L, when the values of R and R_d are invariant. In this simulation, the values of R and R_d are larger than actual values. However, a deviation of the output voltage between the simulated value and the ideal value is only 0.5%~1.5%. Therefore, the influence of the inner resistances on the characteristic of the CV output in the CV mode can be ignored. The load voltage U_{RL} is still thought to be load independent.

In conclusion, by simulating the two topologies obtained above, it is obvious that the resistance of the inductive component has an impact on the CC and CV outputs in WPT systems. In addition, it presents a much larger influence on the CC output with the LCL-LCL topology than the CV output with the LCL-S topology.

IV. CHARGING MODE CONVERSION STRATEGY AND SYSTEM DESIGN

For a battery with a fixed voltage level, it is assumed that its nominal voltage is $U_{bat,n}$. When a battery is under voltage, its voltage is $U_{bat,u}$. At any time during the lithium battery charging process, the charging voltage U_{bat} and the charging current I_{bat} of the battery are dc values. Therefore, the external characteristic of the battery can equal to the variable resistance $R_{bat,eq}=U_{bat}/I_{bat}$.

In the stage of CC charging, the battery is charged at a pre-set current which is constant during the process. In this case, U_{bat} increases when charging time increases. When U_{bat} increases to $U_{bat,n}$, the charging process is transformed to the CV mode. In the stage of CV charging, the charging current is gradually reduced to trickling charging with the charging voltage remaining unchanged until the battery is full. Throughout the entire charging process, the variation of $R_{bat,eq}$ is given by (15).
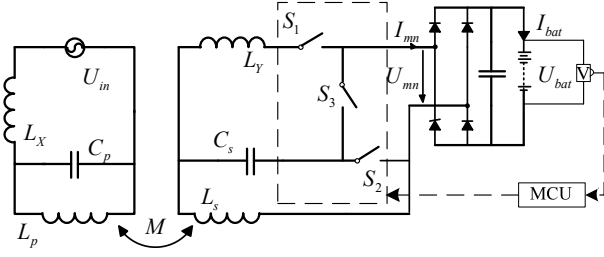
Fig. 7. WPT battery charger.

TABLE III
KNOWN PARAMETERS

Parameter	Theoretical	Experimental
$L_p=L_s=L_X=L_Y=L$	12μH	12μH
M	2.5μH	2.5μH
$U_{bat,n}$	5V	5V
I_{bat}	1A	1A

TABLE II
CONTROL LOGICS FOR SWITCHES

	S_1	S_2	S_3
CC	+	+	-
CV	-	-	+

TABLE IV
CALCULATED PARAMETERS

Parameter	Theoretical	Experimental
U_{in} (V)	26	26
f(kHz)	64.3	65
$C_p=C_s=C$(μF)	0.51	0.5

$$\begin{cases} \dfrac{V_{bat.n}}{I_{bat}} \geq R_{bat \cdot eq} \geq \dfrac{V_{bat}}{I_{bat}} & \text{CCmode} \\ \infty \geq R_{bat \cdot eq} \geq \dfrac{V_{bat.n}}{I_{bat}} & \text{CVmode} \end{cases} \quad (15)$$

Therefore, based on the above analysis, the design of a WPT system can be divided into two parts: the realization of the topological transformation and the setting of the system parameters.

A. Charging Mode Conversion

A battery charger is designed as shown in Fig. 7. The switches S_1, S_2, and S_3 are normally open switches, and they are used to control the switching of the charging mode. These ac switches are all high-frequency single-pole single-throw switches.

The control logics for the ac switches of a WPT system operating between the CC and CV modes are shown in Table II.

In table II, '+' represents the switch on, while '–' represents the switch off. When the system works in the CC mode, S_1 and S_2 are on, and S_3 is off. The battery voltage U_{bat} gradually increases with a prolonged charging time. When the value of U_{bat} reaches $U_{bat,n}$, the WPT battery charger is switched into the CV mode. At this point, S_1 and S_2 are off, and S_3 is on.

B. System Design Procedures

Based on the nominal voltage $U_{bat,n}$ that is already known, the power supply voltage U_{in} used to maintain CV output can be calculated first. This is due to the fact that in the CV mode, the output voltage of the LCL-S topology is not relevant to the system frequency. In order to keep U_{in} constant during the charging process, the angular frequency ω in a WPT system can be calculated according to a pre-set value of the charging current I_{bat} in the CC mode. Finally, the value of the compensation capacitor can be obtained. The steps for doing this are described as follows:

Step 1: The different characteristics of batteries determine that different batteries have different charging parameters. Therefore, according to the nominal voltage $U_{bat,n}$ and the characteristics of a battery, the charging current I_{bat} in the CC mode should be pre-set first.

Step 2: The inductances should be set according to different applications. It is assumed that in this system $L_p=L_s=L_X=L_Y=L$ and the mutual inductance M is given.

Step 3: Calculate the input source voltage U_{in} whose value is constant during the whole charging process. Because the output voltage is an ac voltage, it needs to be rectified by a full-bridge diode rectifier to charge the battery. In addition, each diode in the full-bridge rectifier has the tube voltage drop U_E. The relationship between U_{mn} and U_{bat} is given as:

$$U_{bat} = \frac{\sqrt{2}\pi U_{mn}}{4} - 2U_E \quad (16)$$

By combining (2) with (16), the input voltage can be calculated.

$$U_{in} = \frac{4L(U_{bat,n} + 2U_E)}{\sqrt{2}\pi M} \quad (17)$$

Step 4: In the CC mode, the ac current I_{mn} before rectifying and the pre-set battery charging current I_{bat} satisfy the relationship in (18).

$$I_{bat} = \frac{2\sqrt{2}I_{mn}}{\pi} \quad (18)$$

By combining (14) and (18), with the input voltage U_{in} remaining unchanged, the angular frequency can be calculated as follows:

$$\omega = \frac{4(U_{bat,n} + 2U_E)}{\pi^2 L I_{bat}} + \sqrt{\frac{16(U_{bat,n} + 2U_E)^2}{\pi^4 L^2 I_{bat}^2} - \frac{RR_{bat,eq,n}}{L^2}} \quad (19)$$

Where $R_{bat,eq,n} = U_{bat,n}/I_{bat}$.

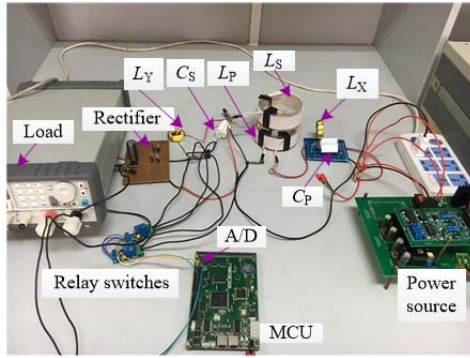Step 5: Based on the angular frequency in (19), the compensation capacitor can be obtained by $C=1/(L\omega^2)$.

Fig. 8. Experiment prototype of a WPT battery charger.

Fig. 9. Charging profile during the whole charging process.

V. EXPERIMENTAL VALIDATION

To verify the above analysis, the known parameters are shown in Table III. A lithium-ion battery is taken as a research object with a nominal voltage $U_{bat,n}$ of 5 V, and the charging current I_{bat} in the CC mode is pre-set to 1 A.

To ensure that the charging current in the CC mode and the charging voltage in the CV mode meet the requirements, by combining with the content of the parameters design in section IV, the other parameters are calculated in Table IV.

When the battery experiences under voltage, the open circuit voltage is set to 3V. The charging current I_{bat} in the CC mode is 1A. Therefore, the initial equivalent resistance $R_{bat.eq}$ is 3Ω. In addition, the increasing load resistance is set as the abscissa. The charging mode is switched by detecting the battery voltage U_{bat}. Once U_{bat}=5V, the topology is changed to realize switching from the CC mode to the CV mode. Experimental prototypes have been built according to the parameters in Tables III-IV. Specifically, the transmitting coil and receiving coil are helical coils with a turn number of 12 and a diameter of 10 cm. The air gap between the transmitting coil and receiving coil is 4cm. The inverter is a full bridge. A full bridge driver UCC3895 drives four IRFP460 MOSFETs. The current probe is 0.1V/A.

In Fig. 8, the battery charging process is simulated by adjusting the electronic load. The voltage signals detected by a voltage sensor are converted into digital signals using an A/D module. Relay switches are controlled by programming in MCU to realize the transformation between the CC and CV modes. The charging profile and measured efficiencies are shown in Fig. 9 and Fig. 10, respectively.

Fig. 9 shows curves of the charging current and charging voltage during the whole charging process. In the CC mode, the simulated charging current is 1 A, and the experimental charging is about 1 A. This indicates that the system designed by Section IV can ensure a constant output current in the CC mode, which is the same as the pre-set one. The battery voltage U_{bat} rises to 5V ($R_{bat.eq}$=5Ω). The operating mode is switched from the CC mode to the CV mode. Then the WPT system enters into the CV mode. When $R_{bat.eq}$ increases, the charging current I_{bat} is gradually reduced, and the charging
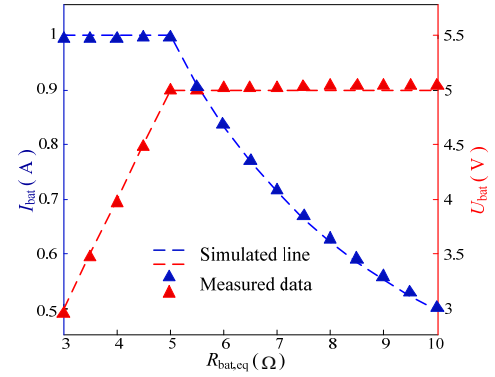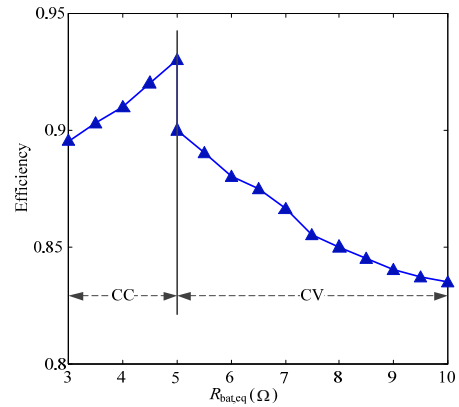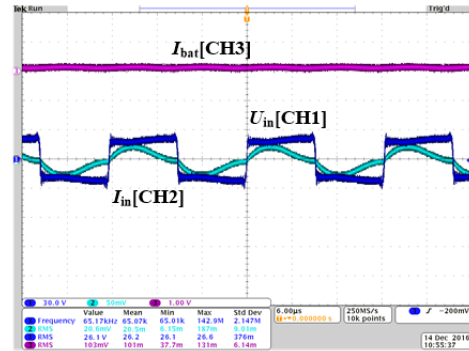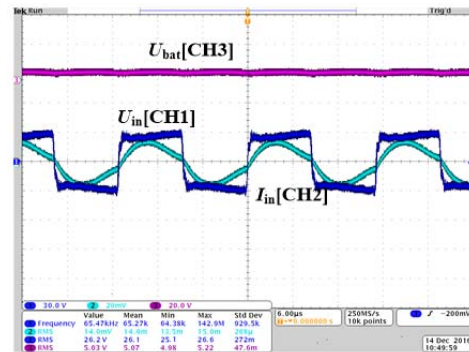

Fig. 10. Measured efficiencies during the charging process.

Fig. 11. Experimental waveforms of U_{in}, I_{in}, and I_{bat} ($R_{bat.eq}$=5Ω in the CC mode).

Fig. 12. Experimental waveforms of U_{in}, I_{in}, and U_{bat} ($R_{bat.eq}$=8Ω in the CV mode).

voltage U_{bat} is kept stable at around 5V. Namely, in the CV mode, by using the design procedures in Section IV, the CV charging can be realized and the output voltage is the same as the battery's nominal voltage. During the whole charging process, the charging current and charging voltage change smoothly. Therefore, the validity of the battery charger and the correctness of system design are verified.

The efficiency from the input to the battery in the whole charging process is shown in Fig. 10. Normally in a WPT system, there is an optimal load corresponding to the highest efficiency. The charging process of a battery is equal to the process of searching for an optimal load in the LCL-LCL topology and the LCL-S topology. In the CC mode, the value of $R_{bat,eq}$ is getting close to the optimal load of the LCL-LCL topology. Therefore, there is an upward trend in terms of the system efficiency. At the moment of the switching charging mode, due to the change of the system topology, the system efficiency drops. While in the CV mode, the value of $R_{bat,eq}$ is moving away from the optimal load of the LCL-S topology. Therefore, a downward trend in terms of efficiency occurs in the CV mode.

Waveforms of the charging current and charging voltage at a certain time of the system, which works in different modes, are shown Fig. 11 and Fig. 12, respectively.

In Fig. 11, $R_{bat.eq}$=5Ω, U_{in}=26.1V, f=65.17kHz and I_{in}=0.206A. At that point, the output current I_{bat} is equal to 1.03A, which is also consistent with the pre-set one. In this case, U_{in} is in phase with I_{in}, which illustrates that the reactive power has been eliminated. Fig. 12 shows waveforms of the input voltage U_{in}, input current I_{in} and output voltage U_{bat} in the CV mode with $R_{bat.eq}$=8Ω. Obviously, U_{in}=26.2V, f=65.47kHz, I_{in}=0.14A and U_{bat}=5.03V. This shows that in practice, the CV output is achieved and kept at 5V. In addition, U_{in} is still in the same phase as I_{in}.

VI. CONCLUSION

In this paper, a WPT system and a switching strategy are designed to realize CC and CV charging for batteries.

(1) Through an analysis of the LCL circuit used at the transmitting side and the selection of a topology at the receiving side, a LCL-LCL topology and a LCL-S topology are designed to realize the CC output and the CV output, respectively. Meanwhile, under the two types of topologies, the input voltage always has the same phase as the input current.

(2) By using the method of the theoretical and simulated analysis, for a LCL-LCL topology considering inner resistances, it is the inner resistances of the transmitting coil and receiving coil that mainly influence the CC output. Meanwhile in the CV mode, the inner resistances have little influence on the CV output. Therefore, in practical applications, the resistances of the transmitting coil and

receiving coil need to be reduced to improve the constancy of the output.

(3) Based on the above analysis, a WPT system which can be switched from the CC mode to the CV mode has been designed in this paper. Meanwhile, the proposed system design procedures can ensure that the charging current in the CC mode and the charging voltage in the CV mode meet the requirements.

REFERENCES

[1] A. Kurs, A. Karalis, and R. Moffatt, "Wireless power transfer via strongly coupled magnetic resonances," *Science*, Vol. 317, No. 5834, pp. 83-86, Jun. 2007.

[2] J. Guo, W. Wang, and H. Liu, "Switching control optimization strategy of segmented transmitting coils for on-road charging of electrical vehicles," *IET Power Electron.*, Vol. 11, No. 9, pp.2282-2288, Sep. 2016.

[3] S. Li and C.C. Mi, "Wireless power transfer for electric vehicle applications," *IEEE J. Emerg. Sel. Topics Power Electron.*, Vol. 3, No. 1, pp. 4-17, Mar. 2015.

[4] L. Tan, J. Guo and X. Huang, "Output power stabilisation of wireless power transfer system with multiple transmitters," *IET Power Electron.*, Vol. 9, No. 7, pp. 1374-1380, Jun. 2016.

[5] J. Zhao, "A general design method of primary compensation network for dynamic WPT system maintaining stable transmission power," *IEEE Trans. Power Electron.*, Vol. 12, No. 31, pp. 8343-8358, Dec. 2016.

[6] H. Liu, L. Tan, and X. Huang, "A topological transformation and hierarchical compensation capacitor control in segmented on-road charging system for electrical vehicles," *Journal of Power Electronics*, Vol. 16, No. 4, pp. 1621-1628, Jul. 2016.

[7] C. H. Hu, Y. S. Shiao, and T. J. Chan, "Development of a universal contactless charger for handheld devices," *IEEE International Symposium on Industrial Electronics, Cambridge*, pp. 99-104, 2008.

[8] D. Kim, J. Park, and H. H. Park, "Generation of magnetic propulsion force and torque for microrobot using wireless power transfer coil," *IEEE Trans. Magn.*, Vol. 51, No. 11, pp 1-4, Jun. 2015

[9] W. X. Zhong, C. Zhang, and X. Liu, "A methodology for making a three-coil wireless power transfer system more energy efficient than a two-coil counterpart for extended transfer distance," *IEEE Trans. Power Electron.*, Vol. 30, No. 2, pp. 933-942, Feb. 2015.

[10] S. Lukic, "Charging ahead," *IEEE Ind. Electron. Mag.*, Vol. 2, No. 4, pp. 22-31, Nov. 2009,

[11] J. T. Boys, G. A. Covic, and Y. Xu, "DC analysis technique for inductive power transfer pick-ups," *IEEE Trans Power Electron*. Vol. 1, No. 20, pp 51-53, Dec. 2003

[12] P. Meyer, P. Germano and Y. Perriard, "Design of a contactless energy transfer system for desktop peripherals," *Proc. the 2010 IEEE Energy Conversion Congress and Exposition*, pp. 1643-1651, 2011.

[13] C. Auvigne, P. Germano, D. Ladas, and Y. Perriard, "A dual-topology ICPT applied to an electric vehicle battery charger," *In Electrical Machines*, pp. 2287-2292, 2012.

[14] K. Huang, S. C. Wong, and C. K. Tse, "Design methodology of a series-series inductive power transfer system for electric vehicle battery charger application," *Proc. the 2014 IEEE Energy Conversion Congress and Exposition (ECCE)*, pp. 1778-1782, 2014.

[15] X. Qu, H. Han, and S. C. Wong, "Hybrid IPT topologies with constant current or constant voltage output for battery charging applications," *IEEE Trans. Power Electron.*, Vol. 30, No. 11, pp. 6329-6337, Nov. 2015

[16] H. Wang, H. Zhang, and Y. Lei, "Analysis on wireless charging circuit characteristic under the hybrid compensation topology," *IEEE International Power Electronics and Motion Control Conference,* pp. 2450-2454, 2016.

[17] D. H. Tran, V. B. Vu, and V. L. Pham, "Design and implementation of high efficiency wireless power transfer system for on-board charger of electric vehicle," *IEEE International Power Electronics and Motion Control Conference*, pp. 2466-2469, 2016.

[18] M. Borage, S. Tiwari, and S. Kotaiah, "Analysis and design of an LCL-T resonant converter as a constant-current power supply," *IEEE Trans. Ind. Electron.*, Vol. 52, No. 6, pp. 1547-1554, Dec. 2005.

[19] K. Song, "Modeling and design of dynamic wireless power transfer system for EV applications," *IECON 2015 - 41st Annual Conference of the IEEE Industrial Electronics Society*, pp. 5229 -5234, 2015.

[20] M. Borage, S. Tiwari, and S. Kotaiah, "LCL-T resonant converter with clamp diodes: A novel constant-current power supply with inherent constant-voltage limit," *IEEE Trans. Ind. Electron.*, Vol. 54, No. 2, pp. 741-746, Apr. 2007

[21] N. Keeling, "Variable tuning in LCL compensated contactless power transfer pickups," *Energy Conversion Congress and Exposition*, pp. 1826-1832, 2009.
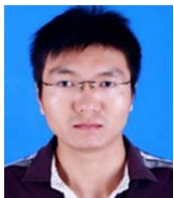
Linlin Tan received his B.S. degree in Electrical Engineering and Automation from the Harbin Engineering University, Harbin, China, in 2008; and his Ph.D. degree in Electrical Engineering from Southeast University, Nanjing, China, in 2014. He is presently working as a Lecturer in the School of Electrical Engineering, Southeast University. Dr. Tan has published more than 20 papers. His current research interests include wireless power transfer, wireless charging for electric vehicles and wireless V2G.

Shulei Pan received his B.S. degree in Mechanical Manufacturing and Automation from the Jiangsu University of Science and Technology, Zhenjiang, China, in 2011. He is presently working towards his M.S. degree in Electrical Engineering at Southeast University, Nanjing, China. His current research interests include wireless power transfer systems.

Changfu Xu received his M.S. degree in Electrical Engineering from Southeast University, Nanjing, China. He has been a Senior Engineer at the Jiangsu Electric Power Company Research Institute, Nanjing, China. His current research interests include intelligent electricity technologies.

Changxin Yan received his B.S. degree in Electrical Engineering from Jiangsu University, Zhenjiang, China, in 2010. He is presently working towards his M.S. degree in Electrical Engineering at Southeast University, Nanjing, China. His current research interests include wireless power transfer systems.

Han Liu was born in Hubei, China, in 1993. He received his B.S. degree from the School of Electrical Engineering, Southeast University, Nanjing, China, in 2014, where he is presently working towards his Ph.D. degree. His current research interests include wireless power transfer technology, power electronics, and EV dynamic wireless charging.

Xueliang Huang received his B.S., M.S. and Ph.D. degrees in Electrical Engineering from Southeast University, Nanjing, China, in 1991, 1994 and 1997, respectively. From 2002 to 2004, he worked as a Post-Doctoral Fellow at the University of Tokyo, Tokyo, Japan. Since 2004, he has been a Professor in the Department of Electrical Engineering, Southeast University. He is the author of four books and more than 150 articles. He is also the creator of more than 40 inventions. His current research interests include wireless power transfer, the analysis of electromagnetic fields, electromagnetic applications, and intelligent electricity technology.